Effects of Suppressed Cyclin B1 Protein Accumulation on Timing of Cell Cycle Events in *Xenopus laevis* Cell-Free Extract System

Owen Blanchard
Department of Biophysics, University of Michigan

Abstract

The cyclin-dependent kinase (Cdk1) oscillator has been widely characterized in bulk xenopus egg extract experiments[1,2]. It was established in a published study that hysteresis, the toggle-like switching of Cdk1 activity by phosphorylation reactions with cyclin B1, drives the cell cycle irreversibly forward[2]. Cyclin B1 is shown to have a minimum concentration threshold that is reached before the progression from interphase into mitosis. Yet the timing of cell cycle events under conditions of suppressed cyclin B1 synthesis have not been hitherto uncovered.

Bulk cytosolic extracts have been a key tool for understanding the early embryonic cell cycle. However, they are far from an in vivo model of Cdk1 temporal dynamics. As a result, water-in-oil microemulsion droplets containing *Xenopus laevis* cytosolic egg extract served as a simplified model of early embryos in this study. This cell-free extract system was applied in conjunction with a Cdk1-EV Forster Resonance Energy Transfer (FRET) Biosensor[3] to uncover the characteristics of Cdk1 dynamics and the progression of cell cycle in the presence of a PEST-tagged cyclin B1. It is strongly suggested from the data collected that the suppression of cyclin B1 accumulation by PEST tagging leads to a delay in the switch from inactive to active Cdk1, thereby prolonging interphase and delaying mitotic entry.

Furthermore, the study employed two separate DNA vector systems, pCS2+ and pcDNA3.1(+), for the purposes of molecular cloning. After the initial round of experimentation, it was noted that the timing of cell cycle events in droplets differs depending on the vector system used to produce the exogenous cyclin B1 mRNA. After a synchronous first peak in Cdk1 activity corresponding to mitosis, pcDNA3.1(+) mRNA-derived droplets exhibited delayed, asynchronous second peaks and drastically increased periods compared to the pCS2+ mRNA-derived counterparts. The inconsistency between vector systems indicates that the pcDNA3.1(+) mRNA is not well-suited for the xenopus egg extract environment and is likely less stable than pCS2+ mRNA.

Chapters

Introduction

The early embryonic cell cycle is distinguished by rapid oscillations. Mature xenopus oocytes are trapped in meiosis metaphase II, in which maturation promoting factor (MPF) is stabilized as cytostatic factor (CSF)[4]. Upon fertilization, intracellular stores of calcium are released that destroy CSF. Anaphase promoting complex/cyclosome (APC/C), an E3 ubiquitin ligase, is activated by the dissociation of emi1 with APC/C activator cdc20[5]. APC/C performs targeted degradation of cyclin B1 that was expressed during metaphase arrest, allowing the cell to progress into interphase. Initiation of mitosis is dependent upon the activation of Cdk1 by the binding of cyclin B1. The activity of cyclin B1-Cdk1 is controlled by a series of interlinked positive feedback loops involving Wee1 and Cdc25[2,6–8]. The activation of Cdk1 corresponds to the activation of APC/C and subsequent degradation of cyclin B1. This prompts the swift deactivation of Cdk1 and mitotic exit[9]. The relationship between cyclin B1 expression and Cdk1 activity was recently investigated by using a newly-developed Cdk1-EV FRET biosensor that allowed researchers to visualize Cdk1 activity and inactivity in the same type of microemulsion droplets used in this study. It was shown that the interaction between cyclin B1 expression and Cdk 1 activity produces a square-shaped trajectory in the phase plane, resulting from their hysteric, switch-like behavior[3]. The bottom, first branch of the loop was characterized by a rate-limited increase in cyclin B1 expression corresponding to a marginal increase in Cdk1 activity. The following branch was described by swift activation of cdk1 with no dependence on cyclin B1. In branch three, Cdk1 activity changed little from its elevated state as cyclin B1 was degraded by APC/C. The final branch exhibited a sharp decrease in Cdk1 activity.

Proline, glutamic acid, serine, and threonine (PEST) enriched amino acid sequences have been proven to target proteins for rapid degradation by proteolysis[10,11]. Many PEST sequences are degraded by ubiquitination by the ubiquitin-26S proteasome[12]. The mechanism by which PEST sequences are recognized for proteolysis are not entirely understood. Nonetheless, PEST sequences are found in a wide range of naturally occurring proteins and have been confirmed to accelerate protein degradation. This study utilizes recombinant DNA technology to place an C-terminus PEST tag on cyclin B1. The PEST sequence serves as a method to continually target cyclin B1 for proteolysis. In doing so, the accumulation of cyclin B1 during interphase is slowed. The resulting effects on the length of interphase and timing of mitotic entry are presented here.

Methods

Key Resources

Reagent or Resource	Source	Identifier
Bacterial Strains		
E.coli DH5α	New England BioLabs	C2987H
BL21 (DE3)	New England BioLabs	C2527H
Chemicals, Peptides, Recombinant Proteins		
KOD One	Toyobo	KMM-101
Ligation High ver.2	Toyobo	LGK-201
2 weight % 008-FluoroSurfactant in HFE7500	Ran Biotechnologies	008-FluoroSurfactant-2wtH-50G
Calcium ionophore A23187	Sigma-Aldrich	C7522
Mineral oil	Macron Fine Chemicals	MK635704
UltraPure™ Agarose	ThermoFisher/Invitrogen	16500100
SYBR™ Safe DNA Gel Stain	Invitrogen	S33102
Gel Loading Dye, Purple (6X), no SDS	New England BioLabs	NEB #B7025
EZBlue Gel Staining Reagent	Sigma-Aldrich	G1041
Critical Commercial Assays		
QIAquick Gel Extraction Kit	QIAGEN	28706
QIAprep Spin Miniprep Kit	QIAGEN	27106
mMESSAGE mMACHINE SP6 Transcription Kit	Ambion	AM1340
mMESSAGE mMACHINE T7 Transcription Kit	Ambion	AM1344
RNeasy Micro Kit	QIAGEN	74004
WillCo-dish® Glass Bottom dishes	WillCo Wells	GWST-5040
Rectangle MiniatureHollow Glass Tubing	VitroCom	5012
QIAquick Gel Extraction Kit	QIAGEN	28706
QIAprep Spin Miniprep Kit	QIAGEN	27106
mMESSAGE mMACHINE SP6 Transcription Kit	Ambion	AM1340
mMESSAGE mMACHINE T7 Transcription Kit	Ambion	AM1344
RNeasy Micro Kit	QIAGEN	74004
WillCo-dish® Glass Bottom dishes	WillCo Wells	GWST-5040
Rectangle Miniature Hollow Glass Tubing	VitroCom	5012
Amicon Ultra-4 10kDa Cutoff Centrifuge Filter	Millipore Sigma	UFC801024
His SpinTrap Prepacked Spin Columns	Cytiva	28401353

Experimental models: Organisms/strains		
Xenopus laevis adult female	NASCO	https://www.enasco.com/c/Education-Supplies/Xenopus-Frogs
Xenopus laevis egg	Xenopus1	N/A
Oligonucleotides		
Morpholino anti-Xenopus-CyclinB1 (ccnb1_a): ACATTTTCCCAAAACCGACAACTGG	Gene Tools, LLC	Custom Order
Morpholino anti-Xenopus-CyclinB1 (ccnb1_b): ACATTTTCTCAAGCGCAAACCTGCA	Gene Tools, LLC	Custom Order
Morpholino anti-Xenopus-CyclinB2 (ccnb2_l): AATTGCAGCCCGACGAGTAGCCAT	Gene Tools, LLC	Custom Order
Morpholino anti-Xenopus-CyclinB2 (ccnb2_s): CGACGAGTAGCCATCTCCGGTAAAA	Gene Tools, LLC	Custom Order
Linker-XhoI-PEST-NotI-F: TCGAGTCCAGCAGCCCTTCTGACTCTGACACTAGTGGATTCAGCTCTGGAGGC	Integrated DNA Technologies	Custom Order
Linker-XhoI-PEST-NotI-R: GGCCGCCTCCAGAGCTGAATCCACTAGTGTCAGAGTCAGAAGGGCTGCTGGAC	Integrated DNA Technologies	Custom Order
Restriction Enzymes		
XhoI	New England BioLabs	NEB #R0146S
NotI	New England BioLabs	NEB #R3189
HindIII	New England BioLabs	NEB #R3104
BamHI	New England BioLabs	NEB #R3136
XbaI	New England BioLabs	NEB #R0145S
ScaI	New England BioLabs	NEB #R3122S
NdeI	New England BioLabs	NEB #R0111S
Recombinant DNA		
pET21a-Cdk1-EV	Yang Lab Previous Study	N/A
pCS2+-CyclinB1-YFP	Yang Lab Previous Study	N/A
pCS2+-CyclinB1	This study	N/A
pCS2+-CyclinB1-PEST	This study	N/A
pcDNA(3.1)+-CyclinB1	This study	N/A
pcDNA(3.1)+-CyclinB1-PEST	This study	N/A

Molecular Cloning and Plasmids

Six plasmids were used in the study and are listed in the Key Resources Table above. All plasmids were designed in Benchling. The sequence maps of the four plasmids constructed in this study are shown in Figure 1 below. Plasmid nomenclature is as follows: the name of the vector is written preceding protein-coding sequences that are written from N-terminus to C-terminus left to right with hyphens in between.

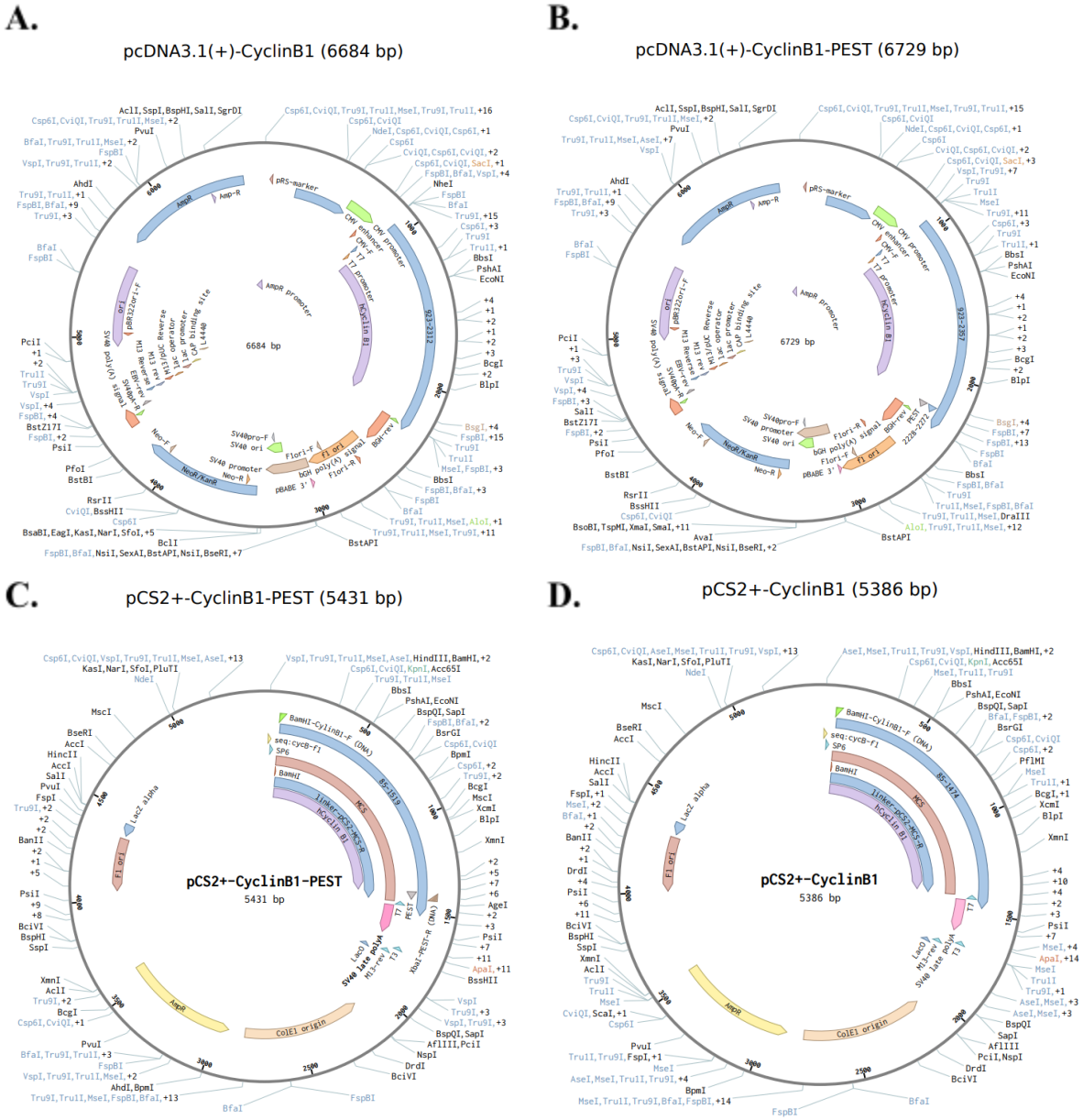

Figure 2. Benchling ® sequence maps of the four plasmids designed and constructed over the duration of the study (A-D). Plasmids above are read from 5' to 3' ends in a clockwise direction.

The construction of pcDNA3.1(+)-Cyclin B1 began with PCR of the human cyclin B1 sequence with forward and reverse primers containing BamHI and XhoI restriction sites respectively. Following PCR, the insert fragment underwent gel electrophoresis to verify the successful amplification. After gel extraction, the fragment and insert were prepared in separate tubes with BamHI, XhoI, and rCutSmart and incubated at 37°C for 20 minutes to create sticky ends suitable for ligation. Another round of gel electrophoresis was performed to ensure the digestion had been completed successfully. 1.0uL of eluted fragment solution, 0.5uL of eluted vector solution, and 1.5uL of Ligation High V2 were mixed and incubated at 16°C for twenty minutes. A 1:2 vector to fragment ligation ratio was chosen to increase the success rate of ligation and thereby transformation. Immediately following ligation, the pcDNA3.1(+)-Cyclin B1 plasmid was then transformed on ice for 20 minutes with 100uL of competent DH5α E. coli. The cells were spread on an LB agar ampicillin plate and incubated at 37°C for ~16 hours. Isolated colonies of cells were then picked from the incubated LB agar plates, placed into LB ampicillin liquid medium, and shaken at 225 rpm in the incubator at 37°C for ~16 hours. The plasmid was then extracted from DH5α E. coli. using a QIAGEN QIAprep Spin Miniprep Kit. Concentration and purity of the eluted samples were then analyzed using a spectrophotometer (DeNovix). Digestion of the plasmid with BamHI and XhoI restriction enzymes was completed, and insertion of the cyclin B1 sequence was validated with gel electrophoresis. The pcDNA3.1(+)-Cyclin B1 samples were sent to Eurofins Genomics LLC for sequencing.

Due to the short length of the PEST sequence (45 base pairs), it was unable to be inserted into pcDNA3.1(+) with the same sticky-end ligation that was performed previously. Instead, two complimentary oligomers comprising of the entire PEST sequence, a TAG stop codon, and the XhoI and NotI cut sites, Linker-XhoI-PEST-NotI-Forward and Linker-XhoI-PEST-NotI-Reverse, were annealed together by incubating at 95°C with annealing buffer (10x: 100 mM Tris-HCl, pH 8.0, 10 mM EDTA, pH 8.0, 1 M NaCl). The pcDNA3.1(+)-Cyclin B1 plasmid was prepared by digestion with NotI and XhoI restriction enzymes, gel electrophoresis, and subsequent gel extraction. The PEST fragment and pcDNA3.1(+)-Cyclin B1 vector plasmid were ligated with Ligation Hi Ver.2 at 16°C for 20 minutes. The pcDNA3.1(+)-Cyclin B1-PEST plasmid was then transformed on ice for 20 minutes with 100uL of competent DH5α E. coli. The same transformation, incubation, miniprep, and sequence protocols for the pcDNA3.1(+)-Cyclin B1 plasmid were performed for pcDNA3.1(+)-Cyclin B1-PEST.

The next steps were to construct pCS2+-Cyclin B1 and pCS2+–Cyclin B1-PEST plasmids. To reduce the chances of a mutation arising from performing PCR amplification on the cyclin B1 and cyclin B1-PEST sequences, the cyclin B1 and Cyclin B1–PEST sequences were simply removed from pcDNA3.1(+)-Cyclin B1 and pcDNA3.1(+)-Cyclin B1-PEST by digestion and inserted into the same multiple cloning site in pCS2+. Transformation, incubation, and extraction of pCS2-Cyclin B1 and pCS2–Cyclin B1-PEST were carried out in the same fashion as their pcDNA3.1(+) counterparts.

Challenges/Limitations

Initially, fluorescent proteins were intended to be added to the four vectors constructed for this study. The goal was to quantify the stability of PEST-tagged cyclin B1 in the xenopus cell-free extract system by recording the intensity of the fluorescent signal of the PEST-tagged cyclin B1 over time compared with the intensity of the untagged cyclin B1. However, there were several challenges that prevented the inclusion of mNeonGreen, mCherry, mScarlet-i, and mVenus sequences into the plasmids.

This project began with an attempt to create pcDNA3.1(+)-Cyclin B1-mNeonGreen-PEST by two and three fragment ligation processes. The three fragment ligation included inserting the sequences for PCR-amplified Cyclin B1-mNeonGreen as well as the PEST linker oligomers in the same step. The two fragment ligation was characterized by the insertion of the PCR-amplified mNeonGreen-Cyclin B1 into the vector and, in a separate ligation step, inserting the annealed PEST linker oligomers into pcDNA3.1(+)-Cyclin B1-mNeonGreen. As suspected, the three fragment ligation failed. The two fragment ligation appeared successful in constructing pcDNA(3.1)-Cyclin B1-mNeonGreen, but the PEST sequence could not be inserted even after multiple attempts with varying insert to vector ratios. If the timeline for the project was longer, more trials of the linker ligation could have been completed, but it was determined that we should try to insert mCherry into pcDNA3.1(+)-Cyclin B1 and perform linker ligation to yield pcDNA3.1(+)-Cyclin B1-mCherry and pcDNA3.1(+)-Cyclin B1-mCherry-PEST.

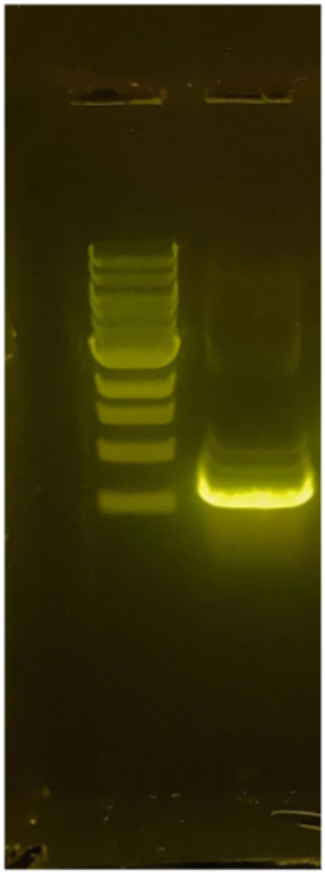

Figure 3. PCR amplification of mNeonGreen DNA sequence. The expected band size for mNeonGreen was 711 bp. The image above shows a 1 kbp ladder (New England BioLabs) in the left lane and the mNeonGreen Sequence in the right lane. The bottom and second-from-bottom bands of the ladder correlate to 500 bp and 1 kbp.

Unfortunately, mCherry was unable to be inserted into the vector. It was determined that the fluorescently tagged cyclin B1 and cyclin B1-PEST were not absolutely crucial for showing the effects of suppressed cyclin B1 accumulation and that more time should be allocated to gathering experimental data with the six completed plasmids listed in the Key Resources Table. While combing through the protocols of the failed attempts at making a fluorescently tagged cyclin B1 and cyclin B1-PEST plasmids, the XhoI-EBFP2-Reverse primer was spotted as a common factor in all of them. An unsuccessful sequence alignment with pCS2-mNeonGreen revealed that the XhoI-EBFP2-Reverse primer was incorrectly manufactured. PCR amplification of the fluorescent proteins appeared normal (Figure 2). However the XhoI-EBFP2-Reverse primer did not include the XhoI restriction site, thereby rendering any attempts to insert a fragment and later

incorporate the PEST sequence impossible. A new XhoI-EBFP2-Reverse primer will have to be ordered for future endeavors.

mRNA Isolation

Before the in vitro transcription, linearization of plasmid DNA by restriction enzyme is required to make transcription machinery attach promoter regions effectively. Therefore, pcDNA3.1(+) plasmids and pCS2+ plasmids were digested with ScaI and NdeI respectively. Linearization of the plasmids followed the same procedure as vector and fragment preparation described above. Restriction enzymes were chosen to have cut sites far from promoter regions, polyadenylated tails, the cyclin B1 sequence, and PEST sequence. Following linearization, in vitro transcription was completed with mMESSAGE mMACHINE SP6 Transcription Kit (Ambion) and mMESSAGE mMACHINE T7 Transcription Kit (Ambion) corresponding to the SP6 forward promoter in the pCS2+ plasmids and the T7 forward promoter in the pcDNA3.1(+) plasmids. Transcription was allowed to run for 2 hours on ice to maximize throughput. Concentration and purity of mRNA was measured with a spectrophotometer (DeNovix).

Cdk1-EV FRET Biosensor

The Cdk1-EV FRET biosensor was developed in a previous study in the Yang Lab[3] modifying a substrate sequence of the ERK FRET biosensor known as EKAREV[13,14]. The Cdk1-EV biosensor is composed of a SECFP, YPet donor–acceptor fluorescent pair[3], the Cdc25C protein sequence as a consensus phosphorylation site for Cdk1 during mitosis[15–17], a WW domain[3], and a flexible 116 amino acid EV linker[3]. Upon phosphorylation by Xenopus Cdk1, Cdk1-EV undergoes a conformational change that allows for the Forster Resonance Energy Transfer to occur between the SECFP donor and the YPet acceptor[3]. The ratio of 'active' YPet signal to 'inactive' SECFP signal indicates the level of Cdk1 activity and implied expression of cyclin B1.

Expression of Cdk1-EV was performed in a very similar fashion to a previous study in the Yang Lab[3]. BL21(DE3) competent cells, induced by 0.4 mM IPTG overnight at 18°C, were used to overexpress and purify the Cdk1-EV protein. Protein purification was performed using a C-terminus histidine tag on Cdk1-EV. Cells were corrected by centrifugation. They were then suspended in ice-cold B-PER Bacterial Protein Extraction Reagent buffer (lysis buffer). The protein samples were then centrifuged through His SpinTrap prepacked spin columns (Cytiva). The target Cdk1-EV proteins were incubated overnight at 4°C. After being washed with wash buffer, the target proteins were eluted with a 4 mL elution buffer (25 mM Na_2HPO_4, 25 mM NaH_2PO_4, 300 mM NaCl, 500 mM Imidazole). All purified proteins were passed through Amicon Ultra-4 10kDa cutoff centrifuge filter (Millipore Sigma). Purity of the eluted protein was checked by CBB staining with EZBlue Gel Staining Reagent (Sigma-Aldrich) and concentration was measured with a spectrophotometer (DeNovix). The proteins were finally aliquoted, flash-frozen, and stored at −80°C.

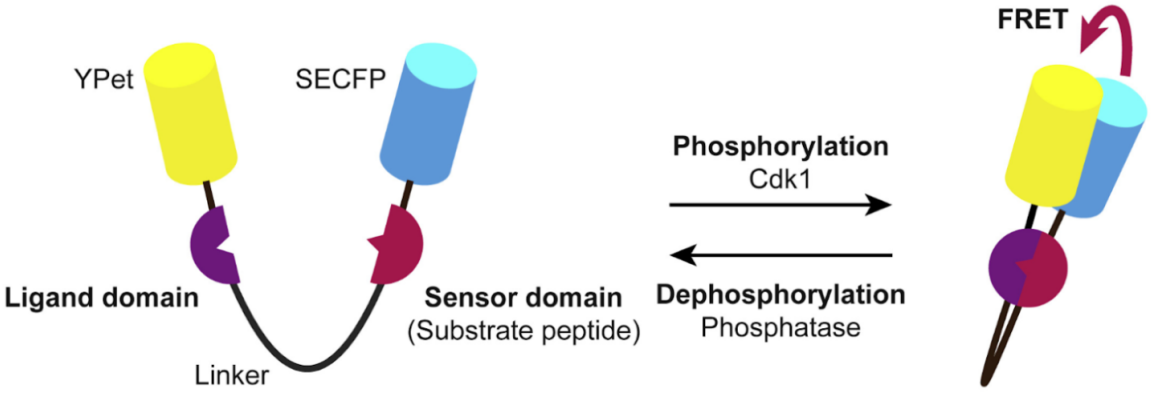

Figure 4. Function of the Cdk1-EV FRET Biosensor[3]. The FRET biosensor undergoes phosphorylation by Cdk1, placing it in an active state that allows for FRET to occur and the emission of photons from the YPet fluorescent protein. Dephosphorylation by antagonistic phosphatases PP1 and PP2a reverts the biosensor back to its inactive state in which photons are emitted from SECFP.

Egg Extract Preparation

Freshly squeezed eggs were collected from *Xenopus laevis*. The jelly coating that surrounds the eggs was removed using a cysteine buffer. The eggs were then activated using calcium ionophore A23187 (200 ng/µL) (Sigma-Aldrich) to simulate the increase in cytosolic calcium and the successive escape from metaphase, passage through anaphase, and entrance into interphase that naturally occurs upon fertilization of the eggs[18]. After activation, the cells were centrifuged in two steps at 20,000×g to separate the cytosolic material. The cytosolic extract and extract mixtures were placed on ice to slow the progression of any cell cycle events, so as to not miss activity before the start of imaging. All conditions were then made from the same batch of cytosolic extract. Each condition was 40 µL in total volume with a 30% dilution of cytosolic extract and included 10 uM added ATP, 1.5 uM Cdk1-EV FRET Biosensor, and extract buffer. Since the objective of the study was to determine how the suppression of cyclin B1 accumulation affects the timing of cell cycle events, it was necessary to deplete the cytosolic extracts of all conditions except for the positive control (egg quality check) of endogenous xenopus cyclin B1/B2 mRNA. To accomplish this, 10 µM morpholinos, antisense oligonucleotides against xenopus cyclin B1/B2 mRNA, were added to the mixture prior to droplets being made in order to ensure consistent morpholino concentrations. A negative control condition with added morpholinos and no exogenous mRNA was created to ensure that there was in fact depletion of the endogenous cyclin B1/B2 mRNA. The experimental conditions all contained 1000 ng of mRNA. Data for this study was gathered from two separate days of experiments. On the first successful day, the validity of the pcDNA3.1(+) mammalian expression vector was evaluated for

the *Xenopus laevis* cell-free extract system. On the second successful day, the effects of PEST-tagged human Cyclin B1 on the timing of cell cycle events compared to untagged human cyclin B1 were investigated.

Challenges/Limitations

The *Xenopus laevis* recruited for this study would typically provide much "healthier" extract. The cell-free droplets would normally undergo 10-15 oscillations in the two day timespan after imaging began in similar, or exactly the same, droplet conditions as were implemented in this study. However, approximately three weeks before experimentation began, lab members noticed that all but a few samples of squeezed eggs had more than 2-4 oscillations. In many cases, no oscillations were observed. At the time, there was no obvious change in protocol that would warrant such a drastic change in extract viability. Initially, it was believed that the buffers used to prepare the extract, such as the extract or wash buffer, had either been made incorrectly or that the stock solutions had expired. This reasoning was ruled out because the date at which reduced oscillation count began preceded the use of new stock solutions and buffers. Due to the short timeline for the project, all of the experiments were conducted with extract experiencing reduced oscillations. The Yang Lab is currently in contact with collaborators that use the *Xenopus laevis* cell-free extract system to resolve the situation.

Droplet Formation in *Xenopus laevis* Cell-Free Extract System

Cell-free droplets were created using the PDMS device designed previously in the Yang Lab[19] (Figure 4). Extract samples and 2% 008-FluoroSurfactant in HFE7500 (Ran Biotechnologies, Inc.) were pumped into their respective ports in the PDMS device through microbore PTFE tubing (ColeParmer). The pressures of the sample (aqueous phase) and fluorosurfactant (oil phase) were individually controlled by an Elveflow OB1 multi-channel flow controller (Elveflow). The pressures ranged from 1.5-2.0 psi and 1.3-1.5 psi for the aqueous phase and oil phase respectively. The range of pressures existed as the result of slight variations in device channels and debris partially blocking fluid flow on occasion. When phases meet each other at the four-way junction shown in Figure 4, turbulent flow is created, allowing for the fluorosurfactant to encapsulate the extract in droplets. The droplets flow from the four-way junction into the device reservoir. Droplets were collected from the reservoir in rectangular glass capillary tubes. The tubes were coated with trichloro (1H,1H,2H,2H-perfluorooctyl) silane to form a superhydrophobic monolayer that could host the droplets[20]. Hundreds of droplets were collected for each condition so as to reduce the impact of variations in biochemical activity between single droplets[21]. The tubes containing droplets were then positioned for imaging in a glass-bottom dish (WillCo Wells) containing mineral oil (Macron Fine Chemicals). Any bubbles and debris were then removed from the mineral oil by viewing the glass-bottom dish under the microscope and pipetting.

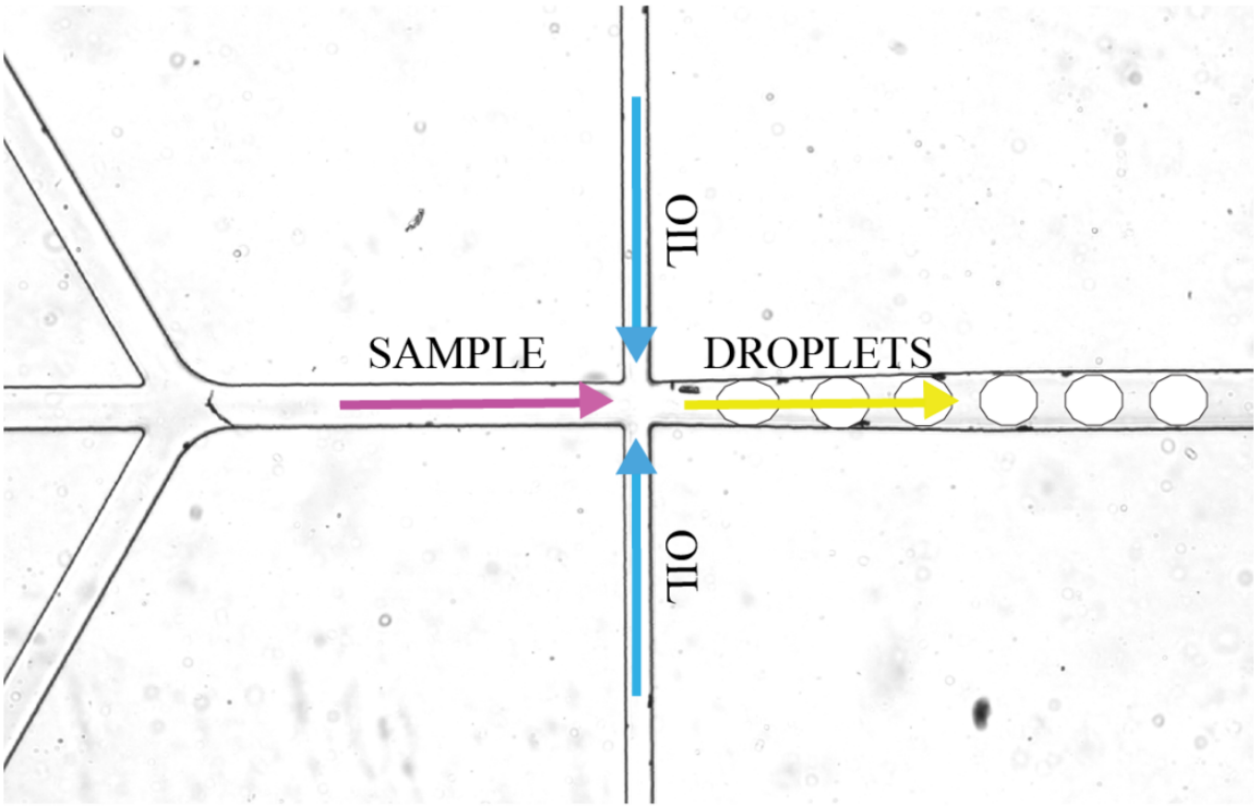

Figure 5. Droplet formation in PDMS microfluidic device. Droplets are represented as white circles. Only one of the three channels on the left were used. The two remaining channels were plugged to maintain fluid pressure and prevent sample escaping the device.

Droplet Imaging

Imaging was completed using the exact same protocol and equipment as in a previous Yang Lab study[3]. Images of the droplets were taken with an IX83 inverted microscope (Olympus) outfitted with a UPlanSApo 4x/0.16 objective lens (Olympus), an ORCA-Flash4.0 V3Digital CMOS camera (Hamamatsu Photonics), an X-Cite Xylis Broad Spectrum LED Illumination System (Exelitas Technologies Corp.), and a motorized XY stage (Prior Scientific Inc.) The microscopy workflow was carried out using open source Micro-Manager software. Channels corresponding to the emission wavelengths of CFP and YFP as well as bright-field were taken for each image. The CFP and YFP channels are consistent with the emission wavelengths of SECFP and YPet regions of the FRET biosensor. Time–lapse image frames were 3-4 minutes apart depending on the number of sample positions and were taken for 30 hours maximum.

Quantification

Image Processing

Image processing was completed using the applicable scripts and methods from the published work in the lab[19]. Droplet tracking was accomplished with MATLAB (MathWorks)) scripts, in which the bright-field frames of the time-lapse images were segmented using a watershed algorithm. The segmentation feature correlation was maximized in between image frames to account for movement of the droplets over the course of the experiment[19].

Data Analysis

The ratio of background-subtracted YPet to SECFP (FRET/CFP) signals was taken as the ratio of active to inactive Cdk1. Since there was no compartmentalization of the droplets in this

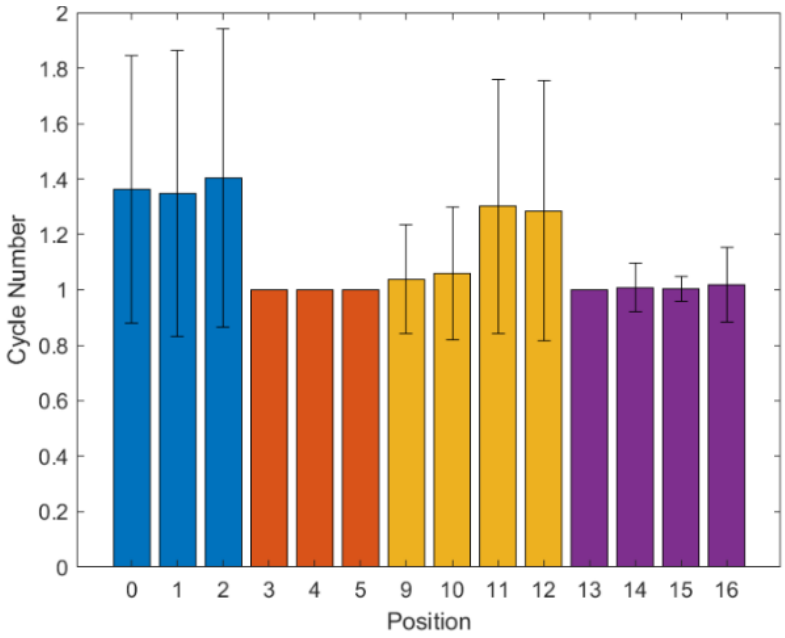

Figure 5. Reduced numbers of oscillations in *Xenopus laevis* cell-free extract system. The average number of cycles (peaks) in positive control (Pos 0-2), suppressed endogenous cyclin B1/B2 mRNA (Pos 3-5), pCS2+-CyclinB1 mRNA (Pos 9-12), and pCS2+-CyclinB1–PEST mRNA (Pos 9-12) conditions are shown as bars. The standard deviations are shown as whiskers. Positions corresponding to suppressed endogenous cyclin B1/B2 mRNA (Pos 3-5) have a standard deviation of approximately zero because almost all droplets had exactly one peak.

study, the FRET and CFP signal intensities were calculated as the whole area averages for each droplet. Taking into account the FRET/CFP ratio value and CFP intensity, peaks and troughs of Cdk1 activity were detected by custom MATLAB scripts from a previous study[3]. An oscillation

period is defined as the space in between one peak and the next, but in many of the droplet conditions, there was only one recorded peak in Cdk1 activity. As a result, the time until the first peak was recorded as the time from which the droplets were first imaged to the time of the first detected peak. All conditions were placed on ice until droplet formation. Therefore, there was not a substantial difference in the starting point at which the droplets were allowed to freely oscillate. There was a trend of linear decay in the FRET/CFP ratio noted in a previous study[3]. Researchers estimated the linear baselines by creating a linear fit to the designated trough values.

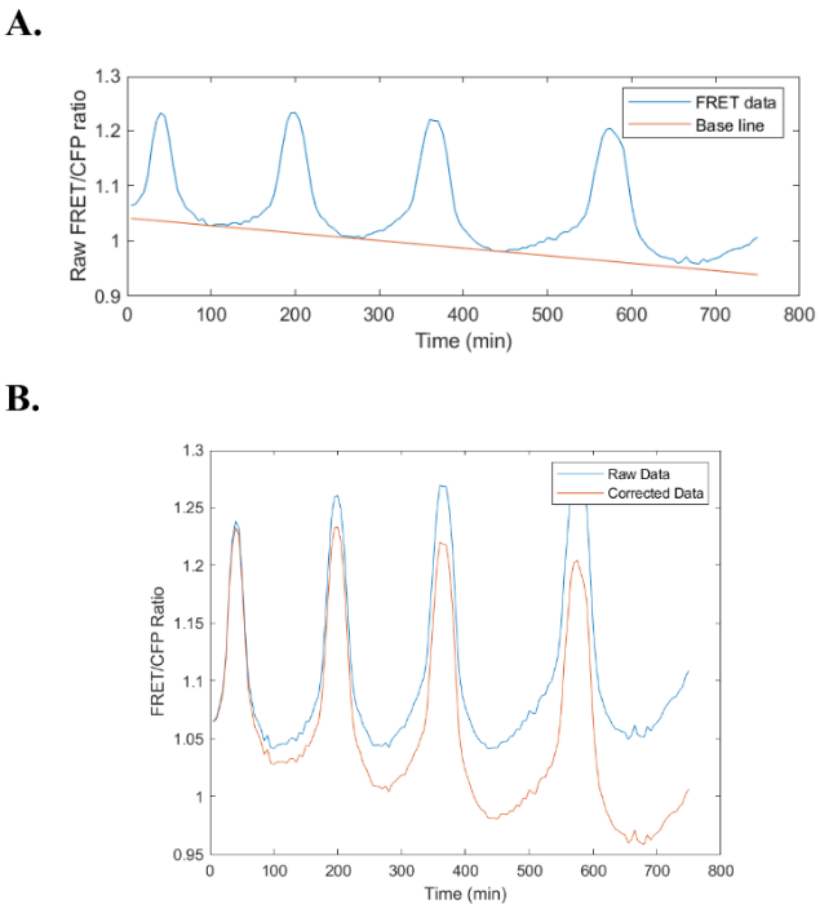

Figure 7. Linear baseline correction of FRET/CFP ration under ideal droplet conditions. Data was taken on the from healthy droplets that were unfortunately not used for any of the experimental conditions in this study. **(A)** The estimated linear baseline traces the troughs of each oscillation and is shown in orange. Raw FRET/CFP ratio is shown in blue. **(B)** Baseline-corrected FRET/CFP ratio is shown in orange. Raw FRET/CFP ratio is shown in blue.

The amplitude of a given peak was calculated by subtracting the linear FRET/CFP baseline at the time point of the peak's maximum from the peak's maximum FRET/CFP ratio value (Figure 5). This definition of amplitude is limited to droplets that express three or more peaks due to how the linear baseline was calculated. The vast majority of droplets do not express three peaks in this study (Figure 6). To avoid falsely classifying the amplitude, the magnitude of a given peak

was calculated by subtracting the peak's maximum FRET/CFP ratio value from the initial FRET/CFP ratio value.

Results

Timing of Cell Cycle Events in the Presence of PEST

After processing the imaging data, the Cdk1-EV FRET biosensor was shown to detect Cdk1 kinase activity effectively (Figure 8). The peaks and troughs of the single line plots in Figure 8 directly correspond to the frames at which droplets were bright and dark in the YFP channel. The incorporation of PEST-tagged cyclin B1 in the xenopus cell-free extract system is characterized by a delayed first peak in Cdk1 activity (Figures 8, 9, and 10). In Figure 8, this is shown by first peaks in the single line plots of pCS2+-Cyclin B1-PEST mRNA droplets occurring around ~250 minutes from the start of imaging, whereas first peaks occur at ~160 minutes in pCS2+-Cyclin B1 mRNA droplets. Figure 10 shows that the time until the first peak in pCS2+-Cyclin B1-PEST mRNA droplets is, on average, ~1.5 fold that of pCS2-Cyclin B1 mRNA droplets. Figure 9 and Figure 10 show that droplets within their respective conditions have similar distributions of first peak time. This is to be expected since both the pCS2-Cyclin B1 mRNA and pCS2-Cyclin B1-PEST mRNA should be equally stable due to the identical 3' polyadenylated tails.

As stated above, the peaks and troughs of Cdk1 activity have been reported to be out-of-phase with cyclin B1 expression in the cell-free extract system[3]. The time at which the rapid increase in Cdk1 activity begins, the transition from the first to second branches of the phase plane trajectory described earlier, is designated by the start of peaks in Figure 8. Assuming that there were no oscillations prior to the start of imaging due to the samples being kept on ice and no major changes in translational efficiency as the result of the PEST sequence only adding 45 base pairs to the mRNA, the increased time until first peak is an strong indication that the PEST sequence very likely caused cyclin B1 to undergo continual degradation by proteolysis throughout the cell cycle. This, in turn, led to the suppression of cyclin B1 accumulation, lengthening the bottom, interphase branch of the phase-plane trajectory and delaying the transition to rapidly increasing Cdk1 activity that occurs in the second branch.

Something to note about Cdk1 activity in all extract conditions, with the exception of the positive control, is the slow decay of Cdk1 activity after approximately 300 minutes into imaging. The bright-field images of pCS2+-Cyclin B1-PEST mRNA droplets, shown in Figure 11, as well as the images of all other conditions besides the positive control (not shown) presented progressively darkening spots in the droplets at 300 minutes, 400, and 800 minutes. These spots were representative of the droplets undergoing cell death and possibly cytoskeletal protein

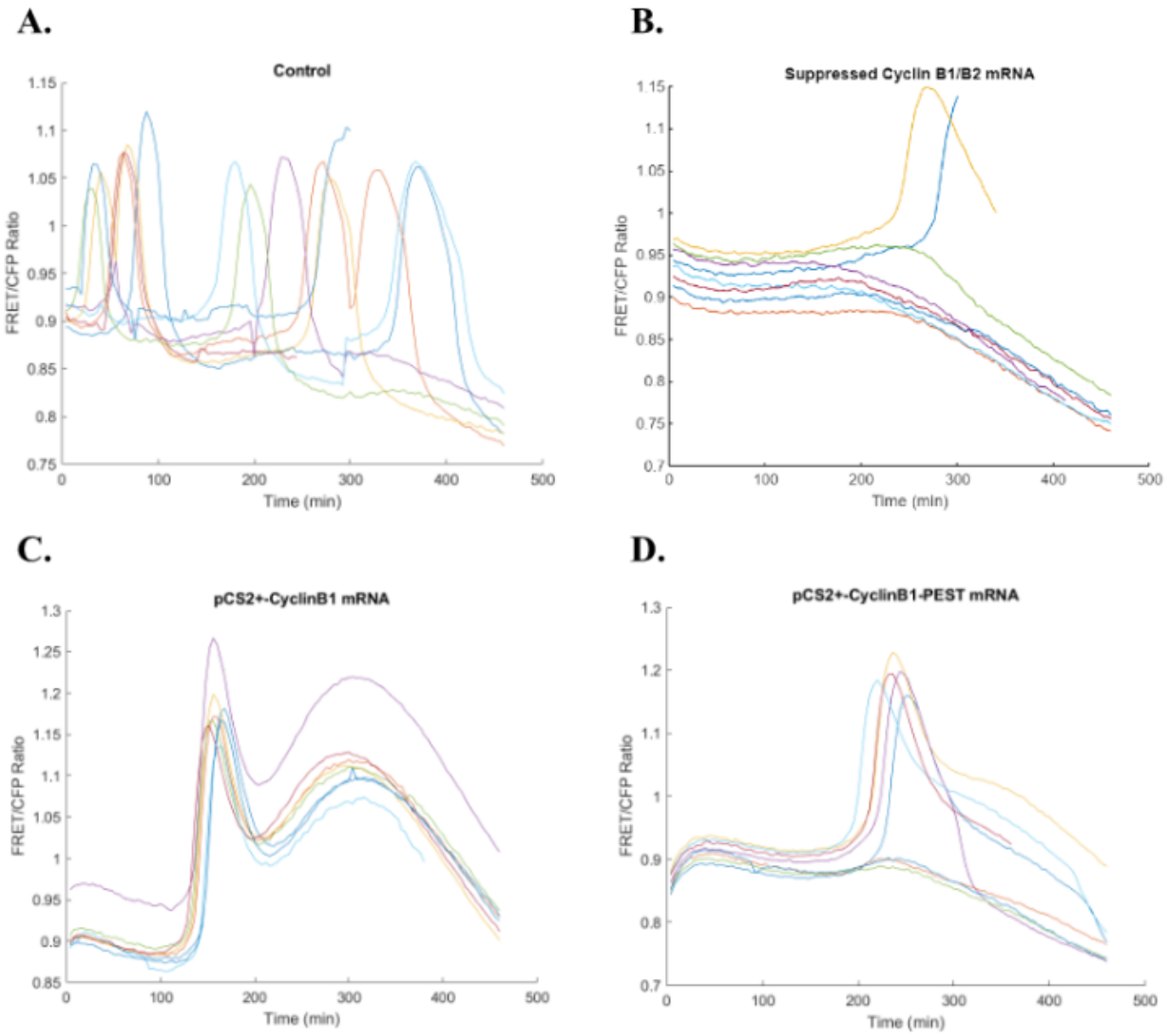

Figure 8. Cdk1–EV FRET Biosensor specifically detects Cdk1 kinase activity in Experiment 2 droplets. Eight droplets were selected at random. The ratios of FRET to CFP emission (y-axes) were measured over 460 minutes (x-axes) for positive control **(A)**, suppressed cyclin B1/B2 mRNA **(B)**, pCS2+-CyclinB1 mRNA **(C)**, and pCS2+-CyclinB1–PEST mRNA **(D)** conditions. Single lines represent the FRET to CFP ratio averaged over the entire area of a single droplet. Colors of single lines were assigned to better distinguish single lines.

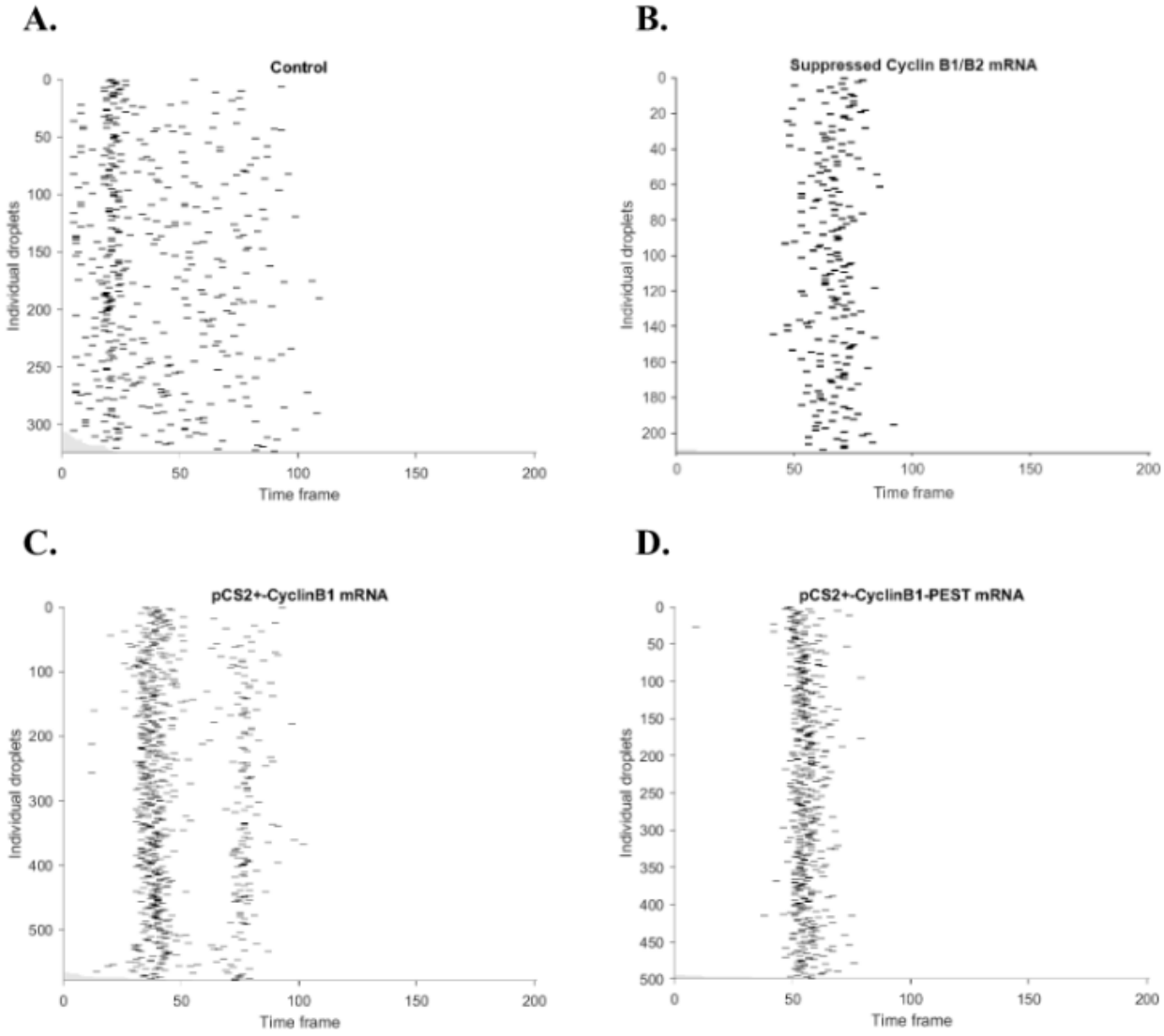

Figure 9. PEST-tagged cyclin B1 halts oscillations by depletion of protein. Raster plots showing registered peak times in positive control **(A)**, droplets with suppression of endogenous cyclin B1/B2 mRNA by antisense morpholinos **(B)**, pCS2+-CyclinB1 mRNA **(C)**, pCS2+-CyclinB1-PEST mRNA **(D)** conditions. Oscillation peaks are shown as black rectangles and correspond to the detected peak of an individual droplet. The gray region of the plots represents the amount of time individual droplets were not being tracked by the MatLab scripts. No information on the oscillation peaks was gathered for the gray regions of the plots.

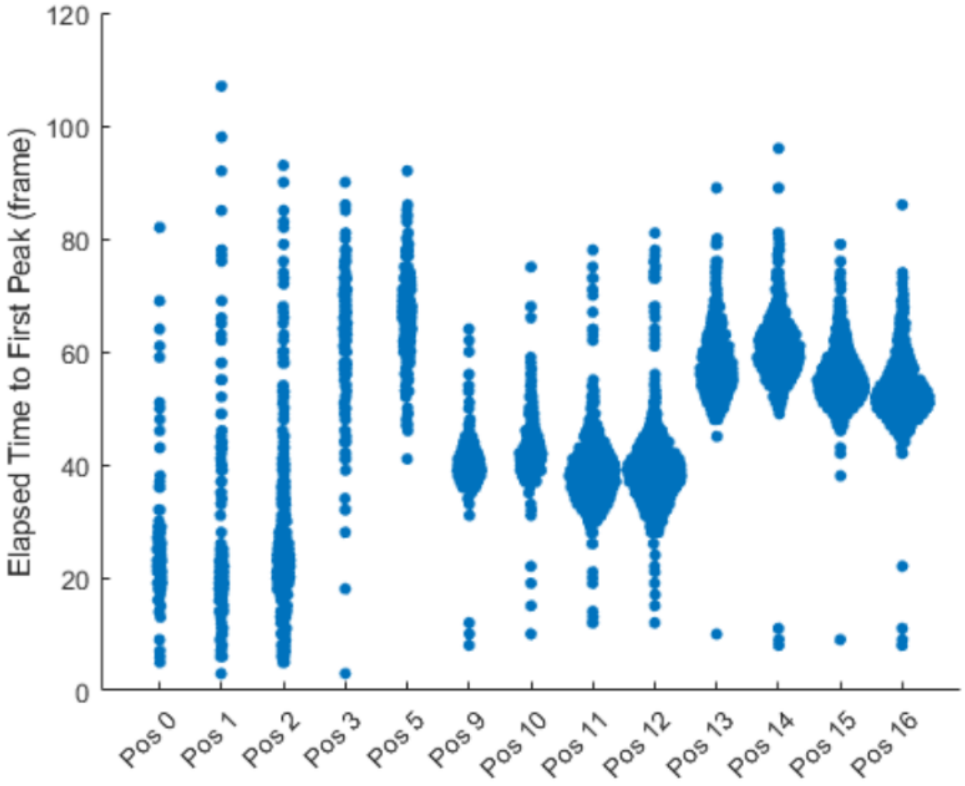

Figure 10. Suppressed accumulation of cyclin B1 prompts delayed first peaks in pCS2+-CyclinB1-PEST conditions. The time from the start of imaging to the first peak is shown for positive control (Pos 0-2), droplets with suppressed endogenous cyclin B1/B2 mRNA (Pos 3-5), pCS2+-CyclinB1 mRNA (Pos 9-12), and pCS2+-CyclinB1–PEST mRNA (Pos 9-12) conditions. Each blue dot represents the time at which an individual droplet had its first peak. The widening of a blue region represents overlapping blue dots.

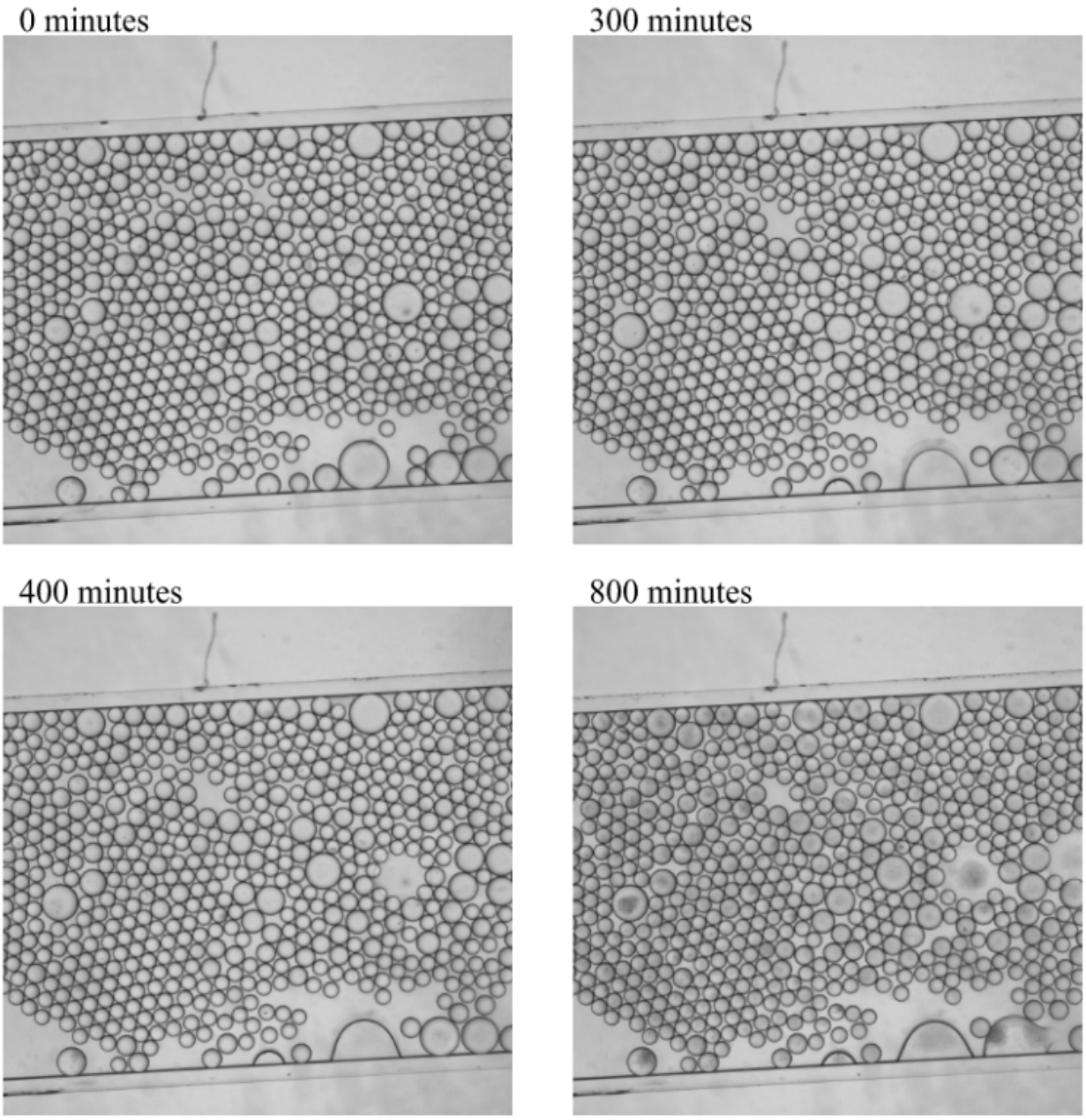

Figure 11. Droplet apoptosis in pCS2+-CyclinB1–PEST conditions. Droplets at the beginning of imaging are relatively transparent. As droplets undergo apoptosis, condensates of cytoskeletal proteins begin to form. Condensates are more easily detected by the eye in large droplets.

pCS2+ and pcDNA™3.1(+) (Invitrogen Vector) Systems

The restriction cut sites corresponding to the enzymes on hand in the laboratory and faster incubation times that would better support workplace logistics for a full-time student initially prompted the use of the pcDNA3.1(+) mammalian expression vector over pCS2+. The first day of experiments that observed oscillations in the positive control group was aimed at

investigating the role of PEST-tagged cyclin B1 by utilizing pCS2+-Cyclin B1-YFP, pcDNA3.1(+)-Cyclin B1, and pcDNA3.1(+)-Cyclin B1-PEST mRNA under endogenous cyclin B1/B2 mRNA translation-suppressed conditions. Upon processing the data, the Cdk1-EV FRET biosensor was shown to detect Cdk1 kinase activity effectively (Figure 12). The peaks and troughs of the single line plots in Figure 12 directly corresponded to the frames at which droplets were bright and dark in the YFP channel.

It was noticeable in the raw imaging data that pcDNA3.1(+)-Cyclin B1 mRNA droplets had a strong, synchronous first peak followed by asynchronous peaks in individual droplets. The observed synchronous peak is visualized in Figure 13. The average time until the first peak from the start of imaging was 80 minutes (16 frames) with a standard deviation of 58 minutes (~ 12 frames) in pCS2+-Cyclin B1-YFP mRNA conditions and 108 minutes (~ 27 frames) with a standard deviation of 138 minutes (~ 28 frames) in pcDNA3.1(+)-Cyclin B1 mRNA conditions. A two-sample t-Test provided a significant p-value<0.001. The average time until the second peak from the start of imaging was 199 minutes (~ 40 frames) with a standard deviation of 69 minutes (~ 14 frames) in pCS2+-Cyclin B1-YFP mRNA conditions and 318 minutes (~64 frames) with a standard deviation of 135 minutes (~27 frames) in pcDNA3.1(+)-Cyclin B1 mRNA conditions. A two-sample t-Test provided a significant p-value <0.001. The differences between pCS2+-Cyclin B1-YFP mRNA and pcDNA3.1(+)-Cyclin B1 mRNA average first and second peak times are 28 minutes (~ 6 frames) and 280 minutes (56 frames) respectively. Figure 8 shows the broadening variation between the first and second peaks in the different vector conditions. Figure 14 shows a general trend in which the period elongates with increasing peak time much more drastically in the pcDNA3.1(+) system than in the pCS2+ system.

The asynchronous nature of second peaks seen in the pcDNA3.1(+)-Cyclin B1 mRNA conditions is potentially the result of limited mRNA availability after significant degradation. Inconsistent translational efficiency of cyclin B1 mRNA would reasonably suppress cyclin B1 accumulation, leading to varied, yet delayed, second peaks in Cdk1 activity (Figure 13). Based on these results, we chose the pCS2+ vector system to evaluate effects of the PEST sequence on the timing of cell cycle events.

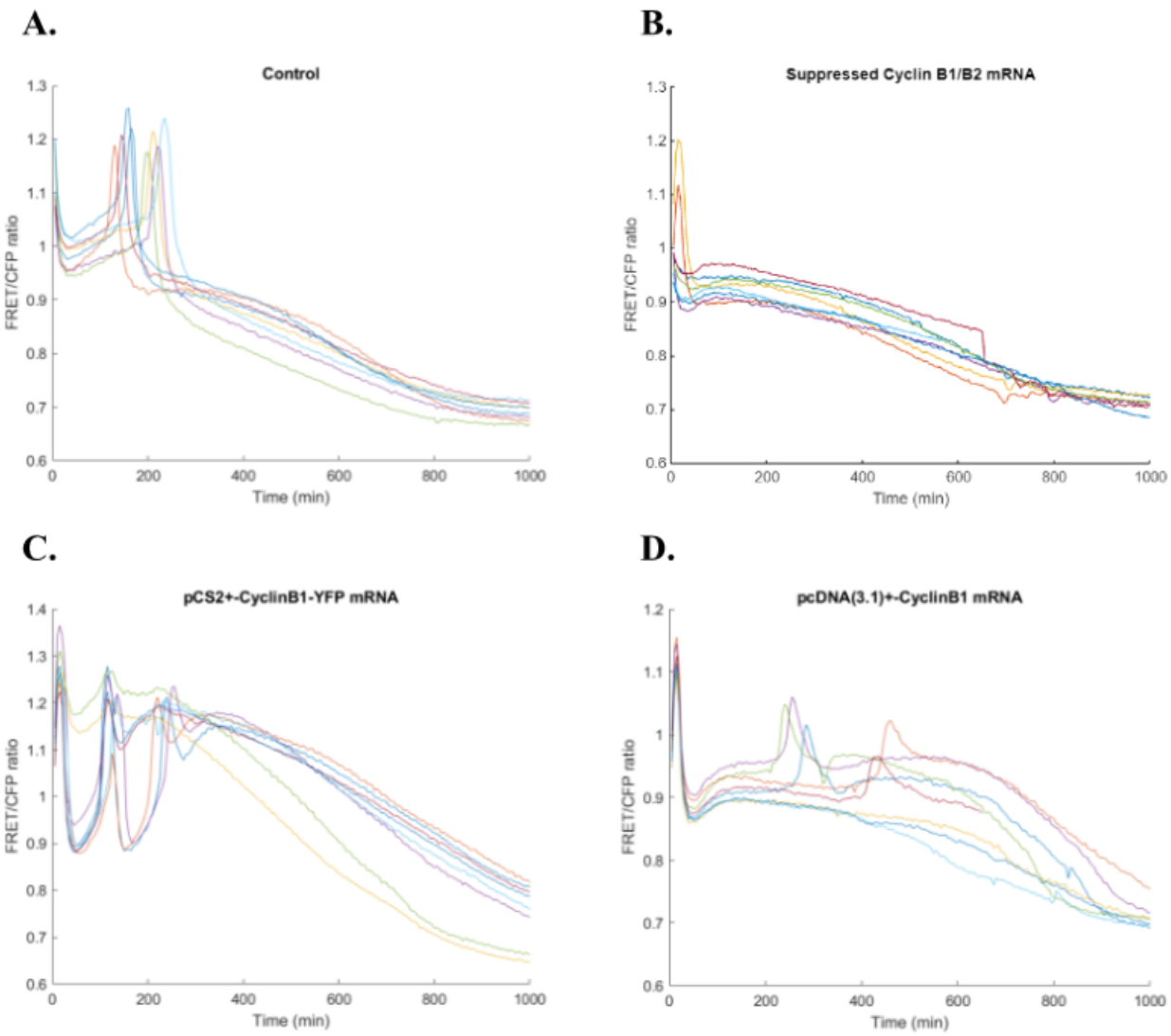

Figure 12. Cdk1–EV FRET Biosensor specifically detects Cdk1 kinase activity in Experiment 1 droplets. Eight droplets were selected at random. The ratios of FRET to CFP emission (y-axes) were measured over 1000 minutes (x-axes) for positive control **(A)**, suppressed endogenous cyclin B1/B2 mRNA **(B)**, pCS2+-CyclinB1-YFP mRNA **(C)**, andpcDNA(3.1)+-CyclinB1 mRNA **(D)** conditions. Single lines represent the FRET to CFP ratio averaged over the entire area of a single droplet. Colors of single lines were assigned to better distinguish single lines.

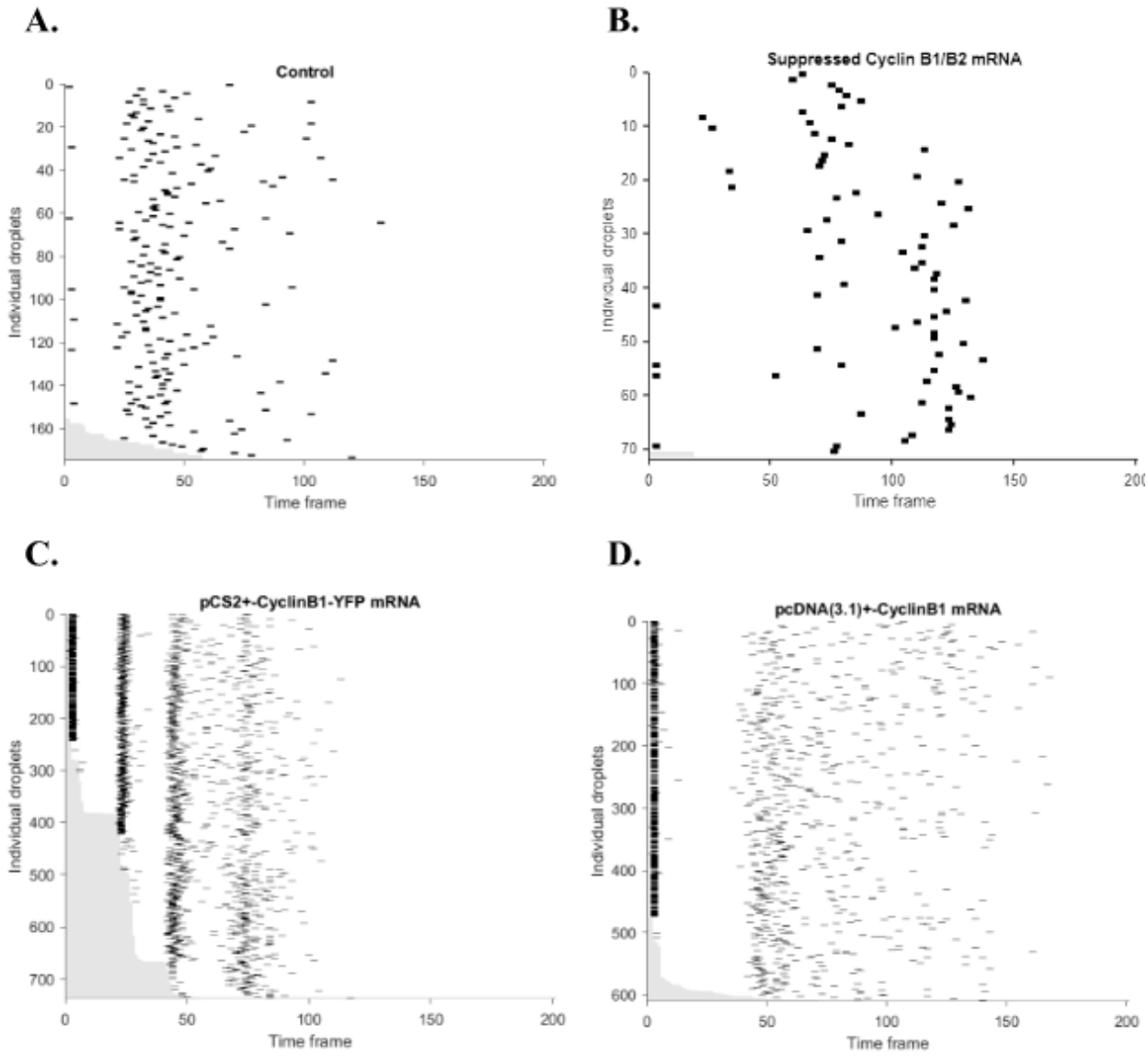

Figure 13. Initial synchronization of first peaks in pCS2+-CyclinB1-YFP mRNA and pcDNA(3.1)+-CyclinB1 mRNA droplets followed by delayed and asynchronous latter peaks in pcDNA(3.1)+-CyclinB1 droplets. Raster plots showing registered peak times in positive control droplets **(A)**, droplets with suppression of endogenous cyclin B1/B2 mRNA by antisense morpholinos **(B)**, droplets containing pCS2+-CyclinB1-YFP mRNA **(C)**, and droplets containing pcDNA(3.1)+-CyclinB1 mRNA **(D)**. Oscillation peaks are shown as black rectangles and correspond to the detected peak of an individual droplet. The gray region of the plots represents the amount of time individual droplets were not being tracked by the MatLab scripts. No information on the oscillation peaks was gathered for the gray regions of the plots.

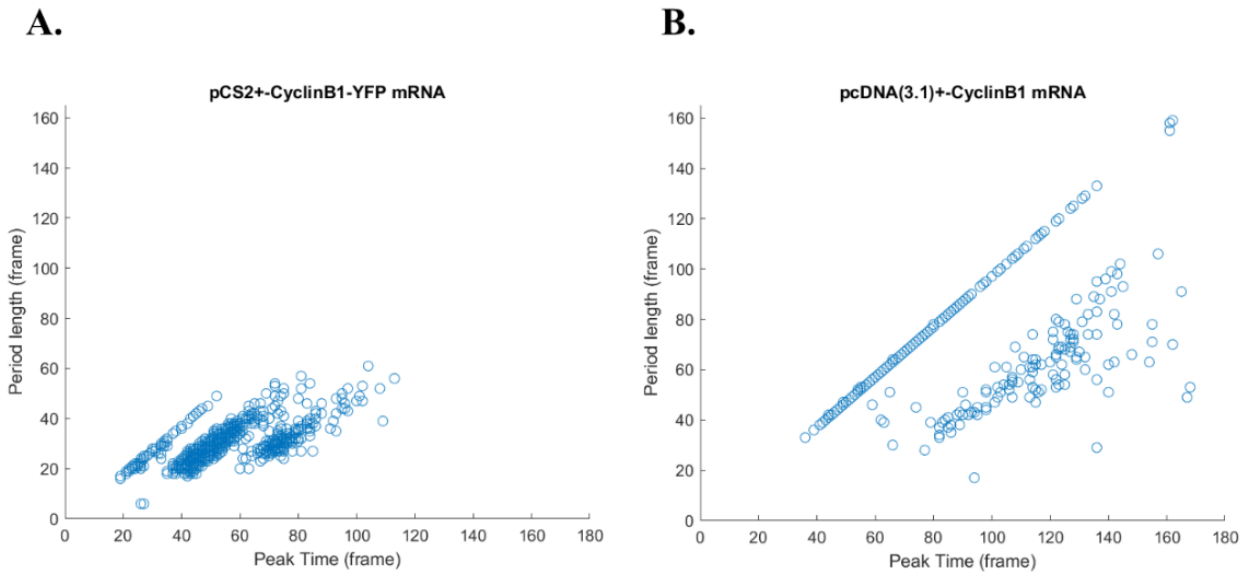

Figure 14. Delayed second peaks in pcDNA(3.1)+-CyclinB1 mRNA-containing droplets reveal increased period length compared to pCS2+-CyclinB1 mRNA. Image frames were taken five minutes apart. If a pcDNA(3.1)+-CyclinB1 mRNA-containing **(A)** droplet or a pCS2+-CyclinB1 mRNA-containing **(B)** droplet had two detected peaks, the image frame at which the second peak occurred (x-axes) and the length of the period (y-axes) were recorded. If no initial or second peak was recorded, the droplet was not included in the plots.

Discussion

Timing of Cell Cycle Events in the Presence of PEST

Given the trend of decreasing Cdk1 activity as well as the visible condensation occurring in a similar imaging time frame for both experimental conditions, it is likely that cell death is halting oscillations prematurely. Consequently, the effect of PEST-tagged cyclin B1 on the lifetime of droplets cannot be commented on in this study. By the time condensation is visible, the droplets had likely already been in the process of apoptosis. This leads to the chance that the broadening of the first peak in pCS2+-Cyclin B1-PEST mRNA conditions and second "peak" in pCS2+-Cyclin B1 mRNA conditions (Figure 8) are marker of cell death instead of typical cell cycle activity. Therefore, we cannot infer how the PEST sequence and continual degradation by protease is affecting mitotic exit from the data presented here.

pCS2+ and pcDNA™3.1(+) (Invitrogen) Vector Systems

A trend of increasing period over time has been observed in previous studies[3,18]. It has been postulated, based on well-established cell cycle models[9,22], that the period elongates in the

extract system as the result of energy depletion[18]. Since this phenomenon of elongating period is present in pCS2+ and pcDNA3.1(+), energy depletion may be at play. However, this does not appear to be the entire story, as is suggested by the disparity in the level of elongation between vector systems. A possible explanation of significantly greater period elongation is rapid degradation of pcDNA3.1(+)-Cyclin B1 mRNA compared to pCS2+-Cyclin B1-YFP mRNA. A lack of Cyclin B1 mRNA concentration due to degradation would intuitively suppress the accumulation of cyclin B1 protein during the bottom branch of the phase plane trajectory described previously.

The pCS2(+) vector system employs an SV-40 3' polyadenylated tail, while the pcDNA3.1(+) vector system includes a Bovine Growth Hormone (BGH) polyadenylated tail (Figure 2). One might propose that decreased translation of cyclin B1 mRNA would also logically suppress accumulation of protein. On the contrary, a study of transient gene expression dependence on the type of poly(A) tail found that in transient transfection of Chinese hamster ovary cells, the BGH and SV40 tails had no statistically significant variation in expression of eGFP[23]. These results suggest that there is likely no difference in the translation of cyclin B1 depending on the vector system. This is supported by the mere 28 minute separation in first peaks between pcDNA3.1(+)-Cyclin B1 and pCS2+-Cyclin B1-YFP mRNA conditions (Figure 13).

At the beginning of the imaging, exogenous mRNA concentrations are equal in all experimental conditions. Additionally, exogenous mRNA concentrations are at a maximum, decreasing from then on. A relatively synchronous initial peak, corresponding to minimal mRNA degradation, implies that cyclin B1 is being translated and accumulated at similar rates regardless of the poly(A) tail in accordance with the study of expression in transient transfection[23]. Major activation of the zygotic genome (zygotic transcription) in *Xenopus laevis* occurs midway through the blastula stage[24]. Therefore, variable mRNA stability is limited by the inability to replace degraded mRNA before this major activation. Short-tailed mRNAs have been shown to be stable in early embryos, and as noted in a previous study[25]. This may be the reason for a population of maily short-tailed mRNAs in early xenopus embryos that is succeeded by a shift to more varied tail lengths as development continues[25]. The artificial early embryonic environment in the cell-free extract system may be more suitable for short-tailed mRNAs. The length of BGH and SV40 ponytails is unknown. Reduced stability in pcDNA(3.1)-Cyclin B1 mRNA may be an indicator of reduced tail length. To verify this is the case, Northern blots or PCR methods would need to be completed on the mRNAs.

Future Directions

There is an ongoing investigation in the Yang Lab into why the microemulsion droplets are experiencing cell death much sooner than would be expected. Also, an effort is underway to diagnose and remedy issues that have been present in the molecular cloning of vectors containing fluorescent proteins. Assuming these projects are successful. The procedures presented in this study will be repeated to first examine the effects of PEST-tagged cyclin B1 in "healthy" egg

extracts and to determine if suppression of cyclin B1 accumulation has an impact on the timing of cell cycle events over multiple oscillations. Furthermore, the difference in that rate of cyclin B1 accumulation between PEST-tagged and unaltered protein will be examined using fluorescent microscopy. Experiments will also be performed using varying ratios of PEST-tagged and unaltered cyclin B1 to comment on the tunability of the oscillator.

Resources and time permitting, further study of the pcDNA3.1(+) vector-derived mRNA in the cell-free extract system using fluorescently labeled cyclin B1 will be employed to monitor mRNA stability. Northern blots or PCR will be performed to identify the lengths of the SV40 and BGH poly(A) tails.

Acknowledgements

I would like to thank Professor Qiong Yang for allowing me to participate in the lab over the past year and for fostering such a supportive and productive research environment. I would also like to thank Postdoctoral Fellow Gembu Maryu for being far and away the most helpful and encouraging mentor I could have asked for. His guidance was invaluable to this project and to my development as a researcher. Additionally, appreciation goes out to PhD candidates Liam Yourston, Franco Tavella, Shiyuan Wang, Minjun Jin, and Usha Kadiyala.

References

1. Murray AW, Kirschner MW. Cyclin synthesis drives the early embryonic cell cycle. *Nature*. 1989;339(6222):275-280. doi:10.1038/339275a0
2. Sha W, Moore J, Chen K, et al. Hysteresis drives cell-cycle transitions in Xenopus laevis egg extracts. *Proc Natl Acad Sci*. 2003;100(3):975-980. doi:10.1073/pnas.0235349100
3. Maryu G, Yang Q. Nuclear-cytoplasmic compartmentalization of cyclin B1-Cdk1 promotes robust timing of mitotic events. *Cell Rep*. 2022;41(13):111870. doi:10.1016/j.celrep.2022.111870
4. Taieb FE, Gross SD, Lewellyn AL, Maller JL. Activation of the anaphase-promoting complex and degradation of cyclin B is not required for progression from Meiosis I to II in Xenopus oocytes. *Curr Biol CB*. 2001;11(7):508-513. doi:10.1016/s0960-9822(01)00145-2
5. Reimann JD, Freed E, Hsu JY, Kramer ER, Peters JM, Jackson PK. Emi1 is a mitotic regulator that interacts with Cdc20 and inhibits the anaphase promoting complex. *Cell*. 2001;105(5):645-655. doi:10.1016/s0092-8674(01)00361-0
6. Heald R, McLoughlin M, McKeon F. Human wee1 maintains mitotic timing by protecting the nucleus from cytoplasmically activated cdc2 kinase. *Cell*. 1993;74(3):463-474. doi:10.1016/0092-8674(93)80048-J
7. Kim SY, Ferrell JE. Substrate Competition as a Source of Ultrasensitivity in the Inactivation of Wee1. *Cell*. 2007;128(6):1133-1145. doi:10.1016/j.cell.2007.01.039
8. Trunnell NB, Poon AC, Kim SY, Ferrell JE. Ultrasensitivity in the Regulation of Cdc25C by Cdk1. *Mol Cell*. 2011;41(3):263-274. doi:10.1016/j.molcel.2011.01.012
9. Yang Q, Ferrell JE. The Cdk1–APC/C cell cycle oscillator circuit functions as a time-delayed, ultrasensitive switch. *Nat Cell Biol*. 2013;15(5):519-525. doi:10.1038/ncb2737
10. Rechsteiner M, Rogers SW. PEST sequences and regulation by proteolysis. *Trends Biochem Sci*. 1996;21(7):267-271. doi:10.1016/S0968-0004(96)10031-1
11. Rogers S, Wells R, Rechsteiner M. Amino Acid Sequences Common to Rapidly Degraded Proteins: The PEST Hypothesis. *Science*. 1986;234(4774):364-368. doi:10.1126/science.2876518
12. Rechsteiner M. Natural substrates of the ubiquitin proteolytic pathway. *Cell*. 1991;66(4):615-618. doi:10.1016/0092-8674(91)90104-7
13. development of an optimized backbone of fret biosensors for kinases and gtpases - Google Search. Accessed April 24, 2023. https://www.google.com/search?q=development+of+an+optimized+backbone+of+fret+biosensors+for+kinases+and+gtpases&oq=Development+of+an+optimized+backbone+of+FRET+biosensors+for+kinases+and+GTPases&aqs=chrome.0.0i512.357j0j7&sourceid=chrome&ie=UTF-8
14. Harvey CD, Ehrhardt AG, Cellurale C, et al. A genetically encoded fluorescent sensor of ERK activity. *Proc Natl Acad Sci*. 2008;105(49):19264-19269. doi:10.1073/pnas.0804598105
15. Aoki K, Kumagai Y, Sakurai A, et al. Stochastic ERK activation induced by noise and cell-to-cell propagation regulates cell density-dependent proliferation. *Mol Cell*. 2013;52(4):529-540. doi:10.1016/j.molcel.2013.09.015
16. Bonnet J, Mayonove P, Morris MC. Differential phosphorylation of Cdc25C phosphatase in mitosis. *Biochem Biophys Res Commun*. 2008;370(3):483-488. doi:10.1016/j.bbrc.2008.03.117

17. Franckhauser C, Mamaeva D, Heron-Milhavet L, Fernandez A, Lamb NJC. Distinct Pools of cdc25C Are Phosphorylated on Specific TP Sites and Differentially Localized in Human Mitotic Cells. *PLOS ONE*. 2010;5(7):e11798. doi:10.1371/journal.pone.0011798
18. A robust and tunable mitotic oscillator in artificial cells | eLife. Accessed April 24, 2023. https://elifesciences.org/articles/33549
19. Sun M, Li Z, Wang S, Maryu G, Yang Q. Building Dynamic Cellular Machineries in Droplet-Based Artificial Cells with Single-Droplet Tracking and Analysis. *Anal Chem*. 2019;91(15):9813-9818. doi:10.1021/acs.analchem.9b01481
20. Qing FL, Ji M, Lu R, Yan K, Mao Z. Synthesis of perfluoroalkyl-containing multifunctional groups compounds for textile finishing. *J Fluor Chem*. 2002;113(1):139-141. doi:10.1016/S0022-1139(01)00495-X
21. Weitz M, Kim J, Kapsner K, Winfree E, Franco E, Simmel FC. Diversity in the dynamical behaviour of a compartmentalized programmable biochemical oscillator. *Nat Chem*. 2014;6(4):295-302. doi:10.1038/nchem.1869
22. Tsai TYC, Theriot JA, Jr JEF. Changes in Oscillatory Dynamics in the Cell Cycle of Early Xenopus laevis Embryos. *PLOS Biol*. 2014;12(2):e1001788. doi:10.1371/journal.pbio.1001788
23. Wang X yin, Du Q jie, Zhang W li, et al. Enhanced Transgene Expression by Optimization of Poly A in Transfected CHO Cells. *Front Bioeng Biotechnol*. 2022;10. Accessed April 25, 2023. https://www.frontiersin.org/articles/10.3389/fbioe.2022.722722
24. Yang J, Aguero T, King ML. The Xenopus Maternal-to-Zygotic Transition from the Perspective of the Germline. *Curr Top Dev Biol*. 2015;113:271-303. doi:10.1016/bs.ctdb.2015.07.021
25. Subtelny AO, Eichhorn SW, Chen GR, Sive H, Bartel DP. Poly(A)-tail profiling reveals an embryonic switch in translational control. *Nature*. 2014;508(7494):66-71. doi:10.1038/nature13007